

# Tomographic Reconstruction of Two-Phase Flows

Han Seo Ko\*

School of Mechanical Engineering, Sungkyunkwan University, 300 Chunchun-dong, Jangan-gu, Suwon, Kyunggi-do 440-746, Korea

Yong-Jae Kim

Graduate School, Department of Mechanical Engineering, Sungkyunkwan University, 300 Chunchun-dong, Jangan-gu, Suwon, Kyunggi-do 440-746, Korea

Tomography has been investigated to observe bubble behaviors in two-phase flows. A bubbly flow and an annular flow have been reconstructed by tomography methods such as an algebraic reconstruction technique (ART) and a multiplicative algebraic reconstruction technique (MART). Computer synthesized phantom fields have been used to calculate asymmetric density distributions for limited cases of 3, 5, and 7 projection angles. As a result of comparison of two tomography methods, the MART method has shown a significant improvement in the reconstruction accuracy for analysis of the two-phase flows.

**Key Words :** Two-phase Flow, Bubbly Flow, Annular Flow, Algebraic Reconstruction Technique, Multiplicative Algebraic Reconstruction Technique

## Nomenclature

$A_j$	: Components of ellipse or circle
$a_j, b_j, c_j$	: Coefficients of components corresponding to location coordinates of center, and major and minor axes
$b$	: Basis function
$C$	: Multiplicative correction vector
$f$	: Actual field
$\hat{f}$	: Gussed or intermediate objective function to be optimized
$\bar{f}$	: Average value of phantom field $f$
$G$	: Gladstone-Dale constant
$J$	: Equally spaced points in $x$ direction
$K$	: Equally spaced points in $y$ direction
$N$	: Number of basis functions
$n$	: Index of refraction
$O_j$	: Height coefficient of $j$ -th basis function
$P$	: Number of projection angles
$q$	: Iteration number

$R$	: Number of ray sums per each projection
$s$	: Coordinate on the projection plane, perpendicular to the ray direction
$t$	: Coordinate parallel to the ray direction
$W$	: Projection matrix
$W_{i,j}$	: Weighting factor of MART
$w_i$	: $i$ -th row of projection matrix
$(x, y)$	: Objective field coordinate
$\langle x, y \rangle$	: Inner product of vectors $x$ and $y$

## Greek Symbols

$\alpha$	: Line-of-sight beam deflection angle
$\Delta$	: Grid spacing
$\Phi$	: Reconstruction error
$\lambda$	: Laser wave length
$\theta$	: Angle of projection
$\rho$	: Density
$\psi$	: Measured projection
$\hat{\psi}$	: Virtual projection of gussed field

## Subscripts

$abs$	: Normalized absolute
$avg$	: Average
$IF$	: Interferometry
$ref$	: Reference condition

\* Corresponding Author,

E-mail : hanseoko@yurim.skku.ac.kr

TEL : +82-31-290-7453; FAX : +82-31-290-5849

School of Mechanical Engineering, Sungkyunkwan University, 300 Chunchun-dong, Jangan-gu, Suwon, Kyunggi-do 440-746, Korea. (Manuscript Received April 8, 2002; Revised October 28, 2002)

*rms* : Normalized rms  
*SP* : Digital specklegram

**Superscript**

\* : Reference field

**1. Introduction**

Two-phase flows, such as bubbly liquid flows, are popular in many industrial processes. The gas-liquid two-phase flow is related to phase-change heat transfer and can be shown in boilers, condensers, dryers, heat pipes, air conditioners, heat exchangers, etc. Thus, the nonintrusive determination of the number, location, and size of the bubbles is increasingly in demand to measure the component fractions and their distributions for analysis of the two-phase flows. Also, this research can be extended to monitor oil behaviors in the refrigeration cycle numerically and experimentally.

The tomography methods are effective tools of the noninvasive and quantitative measurements of the thermal flows (Kak and Slaney, 1987). The line-of-sight optical projection of the two-phase flow is expressed as a ray integral of the refractive index gradient normal to the direction of the incident ray using a digital speckle system (Françon, 1979; Ko et al., 2001) as shown by Fig. 1. The beam deflection angle  $\alpha$  that is projected on the recording plane can be obtained by a ray integral

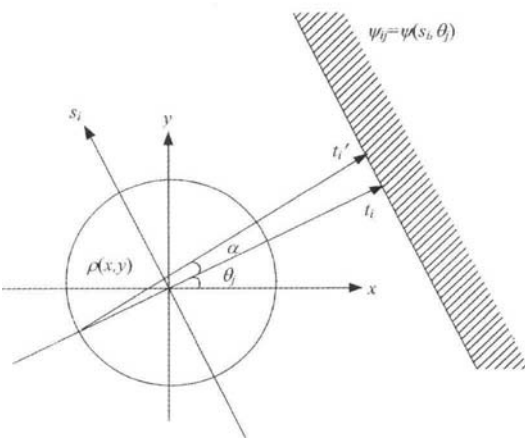


**Fig. 1** Cross-sectional density field  $\rho(x, y)$  and its projection  $\psi_{ij}$  for digital specklegram

of the field density gradient using the Gladstone-Dale relation (Kihm, 1997; Partington, 1953):

$$\psi_{SP}(s, \theta) \cong \alpha = G \int \frac{\partial \rho}{\partial s} dt \quad (1)$$

where  $\psi_{SP}$  is the projection of the digital speckle analysis,  $s$  is perpendicular to,  $t$  is parallel to the incident ray, and  $G$  is the Gladstone-Dale constant.

The optical projection  $\psi_{IF}$  of Mach-Zehnder interferometry is determined by a difference in path length between the reference beam without a phase object and the object beam going through the phase object. The resulting fringe shifts with respect to the undisturbed fringes can be expressed by the ray integration of the density field as follows (Vest, 1979):

$$\psi_{IF} = \frac{1}{\lambda} \int (n - n_{ref}) dt = \frac{G}{\lambda} \int (\rho - \rho_{ref}) dt \quad (2)$$

where  $\lambda$  and  $n$  denote the laser wave length and the refractive index, respectively. Thus, the ray integration of the density gradient determines the beam deflection angle of the digital speckle system while the number of fringe shifts of the Mach-Zehnder interferometry is determined by the ray integration of the density itself. Combining Eqs. (1) and (2) gives (Ko and Kihm, 1999)

$$\begin{aligned} \frac{\partial \psi_{IF}}{\partial s} &= \frac{G}{\lambda} \frac{\partial}{\partial s} \int (\rho - \rho_{ref}) dt \\ &= \frac{G}{\lambda} \int \frac{\partial \rho}{\partial s} dt = \frac{1}{\lambda} \psi_{SP} \end{aligned} \quad (3)$$

Integrating Eq. (3) along  $s$  on the projection plane gives

$$\psi_{IF} = \frac{1}{\lambda} \int \psi_{SP} ds \quad (4)$$

Equation (4) states that an integral of the ray deflection angle from the digital specklegram,  $\psi_{SP}$ , along  $s$  is equivalent to the interferometric fringe shift number  $\psi_{IF}$ . Thus, the results obtained from the Mach-Zehnder interferometry such as the fringe shifts can be compared with those of the digital specklegram such as the deflection angles.

The deflection angle  $\psi_{SP}$  and the fringe shift  $\psi_{IF}$  in Eqs. (1) and (2) must be inverted to reconstruct the true density field  $\rho(x, y)$  and this inversion is called tomography (Fomin, 1998) for

the case of the asymmetric density field. The algebraic reconstruction technique (ART) (Gordon, 1974) and the multiplicative algebraic reconstruction technique (MART) (Verhoeven, 1993) undertake the task of inversion for the two-phase flow in this study. Since Eq. (1) correlating the projection and the density field is non-algebraic, the conventional algebraic reconstruction technique (ART) cannot invert Eq. (1). Thus, the non-algebraic digital specklegram data should be integrated numerically in the projection plane by Eq. (4) to convert the projections into the algebraic interferometric data so that the latter can be converted by the ART or MART. While the tomography was confirmed experimentally for single-phase flows in previous studies (Kastell et al., 1992; Ko and Kihm, 1999; Ko et al., 2001), the ART and MART for the two-phase flow have been examined numerically by using computer-synthesized bubbly and annular flows in this study.

**2. Tomographic Reconstruction Algorithms : Algebraic Reconstruction Technique (ART) and Multiplicative Algebraic Reconstruction Technique (MART)**

For a cross-sectional density field, one can represent the field as a series of basis functions allowing their parameters to be optimally determined. The tomography undertakes the optimization task for the linear case where each basis function is defined by a single parameter (usually its unknown height with a fixed spread). The location of each basis function is given as

$$\hat{f}(x, y) = \sum_{j=1}^{JK} O_j b(x - x_j, y - y_j) \tag{5}$$

where  $\hat{f}$  is an object function that represents the field to be reconstructed,  $b$  is a general form of the basis function located at  $(x_j, y_j)$ , and  $O_j$  is the height coefficient of the  $j$ -th basis function centered at a fixed location of  $(x_j, y_j)$ . The  $(x_j, y_j)$  positions form a rectangular array of  $J$  equally spaced points in the  $x$  direction and  $K$  in the  $y$  direction. Thus,  $JK$  is the total number of co-

efficients to be estimated by the reconstruction algorithm. The use of a smooth basis function such as the cubic B-spline function can accurately represent a relatively smooth object field with far fewer coefficients (unknowns) than with the square-pixel basis function. An optimized set of these unknowns must be found to minimize the deviations between the virtual projection  $\hat{\psi}$  of an intermediate object function and the measured projection  $\psi$  of the actual field  $f$ .

A comparative study (Hanson and Wecksung, 1985) of the choice of basis functions suggests the use of the cubic B-spline, described in the  $x$  variation by

$$b_x(x - x_j) = \begin{cases} \frac{(2\Delta_x - |x - x_j|)^3 - 4(\Delta_x - |x - x_j|)^3}{4\Delta_x^3}, & |x - x_j| < \Delta_x \\ \frac{(2\Delta_x - |x - x_j|)^3}{4\Delta_x^3}, & \Delta_x \leq |x - x_j| \leq 2\Delta_x \\ 0, & |x - x_j| > 2\Delta_x \end{cases} \tag{6}$$

where  $\Delta$  is the grid spacing.  $b_x$  is equal to one at  $x = x_j$ , 0.25 at  $x = x_j \pm \Delta_x$ , 0 at  $x = x_j \pm 2\Delta_x$  and thereafter. The  $y$  variation  $b_y$  is similar, and the two-dimensional basis function is the product of the two, i.e.,  $b(x - x_j, y - y_j) = b_x(x - x_j) \times b_y(y - y_j)$  as shown by Fig. 2. All of the ART and MART results in this research use the cubic B-spline basis function.

The projected ray sum  $\psi_i$  can be obtained as follows :

$$\psi_i = \sum_{j=1}^{JK} O_j \int b(x - x_j, y - y_j) dt \tag{7}$$

where  $i = 1, 2, \dots, PR$  is the total number of ray sums for the number of equally angled projec-

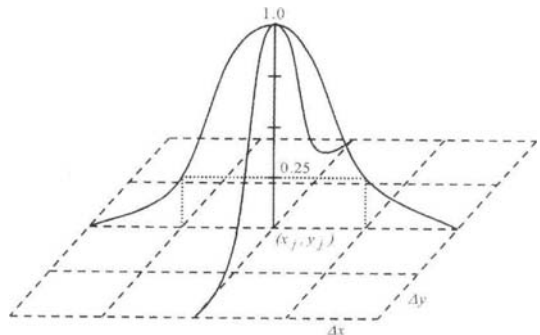


**Fig. 2** Cubic B-spline basis function

tions  $P$ , and the number of ray sums per each projection  $R$ . Equation (7) can be expressed in matrix form as follows :

$$\psi = WO \tag{8}$$

where  $\psi$  is the measurement ray sum vector,  $W$  is the projection matrix, and  $O$  is the object vector to be reconstructed. Solving this set of  $PR$  linear algebraic equations (one equation for each measured ray sum) is the goal of the series-expansion technique such as the ART or MART in  $JK$  unknowns.

The ART algorithm is the basically iterative solver of systems of linear equations (Eq. (8)) adapted to the particular problem of tomographic reconstruction for an object vector  $O$ . The ART uses the feedback information on the deviation of the virtual projection from the measured projection and iteratively optimizes the object coefficient vector  $O$  by an algebraic updating as follows :

$$O^{q+1} = O^q + \frac{\psi_i - \langle w_i, O^q \rangle}{\left( \sum_{j=1}^{JK} w_{i,j} \right)^2} w_i, \quad \sum_{j=1}^{JK} w_{i,j} \neq 0 \tag{9}$$

where  $\langle x, y \rangle$  denotes the inner product of vectors  $x$  and  $y$ ,  $q$  indicates the iteration number,  $w_i$  is the  $i$ -th row of the projection matrix, and  $\psi_i$  is the corresponding measured ray sum. If  $\sum_{j=1}^{JK} w_{i,j} = 0$ ,  $O$  is left unchanged. This algorithm performs the iteration on a ray-by-ray basis until convergence is reached. The object coefficients are enforced at each iteration by setting coefficients that are less than zero after an iteration step to zero. The initial object  $O^0$  for all ART results in this research is a  $JK$ -dimensional zero vector.

Equation (8) can be expressed by the use of the matrix equation as follows :

$$\langle w_i, O \rangle = \begin{bmatrix} \hat{\psi}_1 \\ \hat{\psi}_2 \\ \vdots \\ \hat{\psi}_{PR} \end{bmatrix} = \begin{bmatrix} w_{11} & w_{12} & \cdots & w_{1JK} \\ w_{21} & w_{22} & \cdots & w_{2JK} \\ \vdots & \vdots & \ddots & \vdots \\ w_{PR1} & w_{PR2} & \cdots & w_{PRJK} \end{bmatrix} \begin{bmatrix} O_1 \\ O_2 \\ \vdots \\ O_{JK} \end{bmatrix} \tag{10}$$

where the first matrix denotes the virtual projection from calculation, the second matrix is termed

the projection matrix, and the third is the object matrix to be reconstructed iteratively. Thus, the numerator of Eq. (9), the deviation between the virtual projection  $\hat{\psi}_i$  and the measured projection  $\psi_i$  of the actual field, can also be written from Eq. (10):

$$\psi_i - \langle w_i, O^q \rangle = \psi_i - \hat{\psi}_i \tag{11}$$

where  $i=1, 2, \dots, PR$ . The coefficients of the projection matrix for the case of the square-pixel basis function are all zero and one. If the ray passes through a square-pixel, then the value of the coefficient of the square-pixel is one. Otherwise, it is zero. However, the coefficients of the projection matrix for the cubic B-spline basis function have all different values by Eq. (6) depending on the distance from the fixed location  $(x_j, y_j)$ . Thus, the cubic B-spline basis function is advantageous for the relatively complex object.

Multiplicative algebraic reconstruction technique (MART) differs from the ART only in the way the deviation between the virtual projection and the measured projection  $\hat{\psi}_i$  is distributed among the object coefficients. The MART uses an element  $C_j$  of the multiplicative correction vector  $C$  as follows :

$$O_j^{q+1} = C_j^q O_j^q$$

$$C_j^q = \begin{cases} 1 - 0.5 W_{i,j} \left( 1 - \frac{\psi_i}{\hat{\psi}_i} \right), & \hat{\psi}_i \neq 0 \\ 1, & \text{otherwise} \end{cases} \tag{12}$$

where  $q$  denotes the  $q$ -th iteration and the normalized weighting factor  $W_{i,j}$  is equal to  $w_{i,j}/w_{\max}$  where  $w_{\max}$  is the largest element of the projection matrix  $W$ . One advantage of using MART is to ensure a non-negative object field in reconstructing non-negative scalar.

Note that these algorithm updates, in principle, are possible only for algebraic projections in which the ray integration of the field directly gives the projection data, such as in interferometry (Eq. (2)). Therefore, for the digital specklegram the ray sum must be changed from  $\psi_{SP}$  to  $\psi_{IF}$  by Eq. (4) and the ART and MART must also be modified for the speckle projections.

### 3. Phantom Reference Fields and Reconstruction Errors

The ART and the MART are investigated using two different computer synthesized phantom density fields to reconstruct the two-phase flows. The first one is called the annular flow expressed by

$$f(x, y) = \begin{cases} 0, & [x^2 + (y - 0.05)^2]^{1/2} \leq 0.4 \\ 1, & \text{otherwise} \end{cases} \quad (13)$$

which constructs one big gas bubble in a circular liquid flow as shown by Fig. 3(a). The  $x$  and  $y$  axes have been fixed from  $-0.5$  to  $0.5$  for this normalized phantom density field. Although the real two-phase flow is not so realistic, the tomography has been developed initially to reconstruct the density distribution of the relatively simple

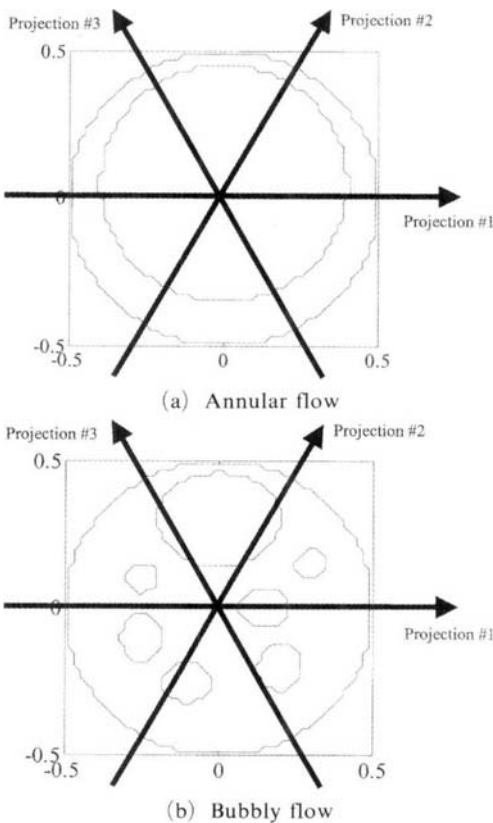


**Fig. 3** Computer synthesized two-phase phantom fields including projection angles

and slow two-phase flow such as the synthesized phantoms and it can be modified to calculate the actual case on the basis of this study.

The second phantom is composed of a set of seven bubbles in the two-phase flow. Individual bubble boundaries are described by ellipses or circles as follows:

$$f(x, y; A_j) = \begin{cases} 0, & \left(\frac{x-x_j}{a_j}\right)^2 + \left(\frac{y-y_j}{b_j}\right)^2 \leq c_j \\ 1, & \text{otherwise} \end{cases} \quad (14)$$

where  $A_j = (x_j, y_j, a_j, b_j, c_j)$ , whose components correspond to the location coordinates of the center and the major and minor axes of the ellipse or the circle. Thus,  $A_j$  of the reference phantom is described as follows (Fig. 3 (b)):

$$\begin{aligned} A_j^* &= (A_1 : A_2 : A_3 : A_4 : A_5 : A_6 : A_7) \\ &= (0.0, 0.3, 0.2, 0.16, 1.0 : 0.3, 0.15, 1.0, 1.0, 0.0025 : \\ &\quad 0.15, 0.0, 0.08, 0.07, 1.0 : 0.2, -0.2, 0.07, 0.08, 1.0 ; \\ &\quad -0.1, -0.25, 0.08, 0.07, 1.0 ; \\ &\quad -0.25, -0.1, 0.07, 0.08, 1.0 ; \\ &\quad -0.25, 0.1, 1.0, 1.0, 0.0025) \end{aligned} \quad (15)$$

where the superscript **\*\*** refers to the reference field. The  $A_2$  and  $A_7$  have been synthesized as the circles while the others are ellipses. The normalized field impedance is 0 for the region inside the bubble and 1 for liquid outside the bubble. The annular and the bubbly flows usually appear in the two-phase flow for the case of the high bubble velocity (relatively faster than liquid velocity) and the low bubble velocity, respectively as shown in Fig. 4. As the heat is added more or the velocity of the bubble increases compared with the liquid velocity, the bubbly flow can be changed into the annular flow.

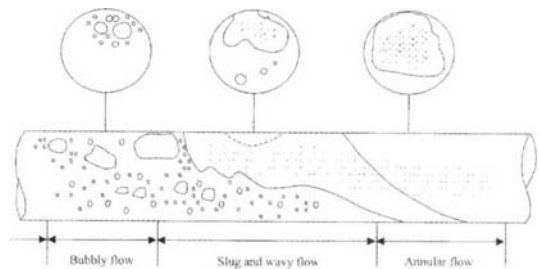


**Fig. 4** Schematic of two-phase flows in horizontal pipe

Three different error measurements are used in this research. The first is the average error of the reconstructed object function  $\hat{f}$  and the reference phantom function  $f$  (Ko et al., 1997):

$$\Phi_{avg} = \frac{\sum_{j=1}^{JK} |f(x_j, y_j) - \hat{f}(x_j, y_j)|}{JK} \quad (16)$$

where  $JK$  is the total number of the basis functions used to conform to the reconstructing object functions. The second is a normalized rms error:

$$\Phi_{rms} = \sqrt{\frac{\sum_{j=1}^{JK} [f(x_j, y_j) - \hat{f}(x_j, y_j)]^2}{\sum_{j=1}^{JK} [f(x_j, y_j) - \bar{f}]^2}} \quad (17)$$

where  $\bar{f}$  is the average value of the phantom field  $f$ . The normalized rms error is large if there are a few large errors in the reconstruction. The third one is a normalized absolute error:

$$\Phi_{abs} = \frac{\sum_{j=1}^{JK} |f(x_j, y_j) - \hat{f}(x_j, y_j)|}{\sum_{j=1}^{JK} |f(x_j, y_j)|} \quad (18)$$

which emphasizes the effect of many small errors. Note that these three errors measure the reconstruction quality based on the comparison between the reconstructed field (object function) and the true field (phantom function) (Liu et al., 1989). In a real experiment, however, the true field is unknown and the quality of reconstruction is only measured by comparing the virtual projection  $\hat{\psi}$  against the measured projection  $\psi$ .

#### 4. Results and Discussion

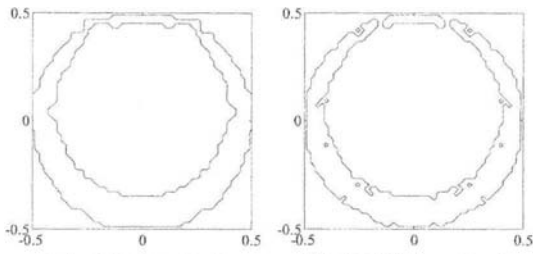
The two reconstruction algorithms, the ART and MART were used to reconstruct the two phantom fields under the interferometric projections since the digital speckle projections can be converted to the interferometric projections by Eq. (4). For the annular flow each projection consists of 300 rays ( $R=300$ ); the object field is described by  $50 \times 50$  cubic B-spline basis functions ( $N=2500$ ). The number of the basis function was varied to test different cases. The resolution was not acceptable for the density distribution of the two-phase flow of the smaller number

of the basis functions than 2500. If the number of the basis function increases, the number of the projected data should be increased to obtain the proper results. Thus, the number of the basis function has been fixed to be 2500 for this number of the projected data to calculate the accurate results. For the case of the bubbly flow each projection consists of 500 rays ( $R=500$ ) and the number of basis functions is  $N=50 \times 50=2500$ . When the iteration exceeds the optimum iteration steps, artifacts may violate the convergence resulting in gradually increasing errors (Decker, 1993). Thus, the calculations are ceased when the minimum is reached for the discrepancy between the reconstructed field and the phantom field. Because the field is asymmetric, more than one projection angle are required to reconstruct the density distribution accurately. Thus, the reconstruction calculations were performed with 3, 5, and 7 equally angled projections ( $P=3, 5, \text{ and } 7$ ) within  $180^\circ$ . For example, the interval of the projection angle for the case of 3 projections is  $60^\circ$  as shown in Fig. 3.

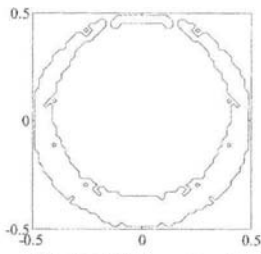
Although the results of the ART and MART show some errors for the reconstruction of the annular flow under 3 projections (Figs. 5(a) and (b)), the ART and MART reconstruct the annular flow precisely under 5 and 7 projections because of the simplicity of the flow shape as shown in Figs. 5(c) to (f). Under 3 projections, which may be regarded as the minimally required projections to perceive an asymmetric object no matter how simple the shape, the MART result shows better reconstruction than that of the ART as shown in Table 1. The multiplicative reconstruction algorithm shows the advantage for the two-phase flow that has simply two density values for liquid and gas because the updating method of the MART is more appropriate for the two-phase flows than that of the ART. From Fig. 5, the number of the projection angles is unnecessarily large for the case of 7 projections because the error of the case of 5 projections already shows zero percent as shown in Table 1. Thus, the required number of the projection angle can be less than 5 for this kind of the simple-shaped flow.

**Table 1** Comparison of reconstruction errors between MART and ART

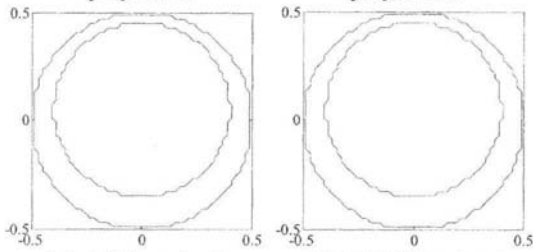
Number of projections	Phantom field	Reconstruction Technique	$\Phi_{avg}(\%)$	$\Phi_{rms}(\%)$	$\Phi_{abs}(\%)$
3	Annular	MART	1.96	7.35	3.69
		ART	3.04	11.45	15.29
	Bubbly	MART	10.16	41.36	17.80
		ART	12.15	51.54	21.30
5	Annular	MART	0.00	0.00	0.00
		ART	0.00	0.00	0.00
	Bubbly	MART	1.12	4.55	1.96
		ART	3.04	12.49	5.33
7	Annular	MART	0.00	0.00	0.00
		ART	0.00	0.00	0.00
	Bubbly	MART	0.00	0.00	0.00
		ART	1.60	6.55	2.80



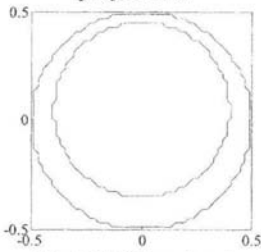
(a) ART under 3 projections



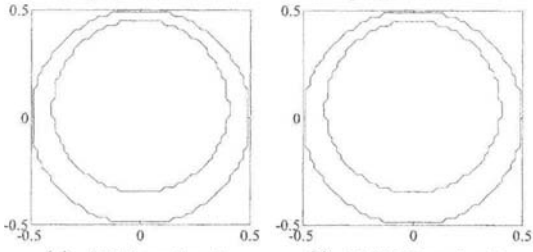
(b) MART under 3 projections



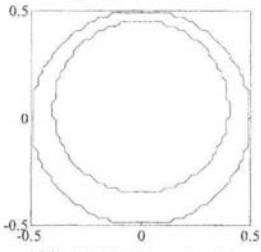
(c) ART under 5 projections



(d) MART under 5 projections

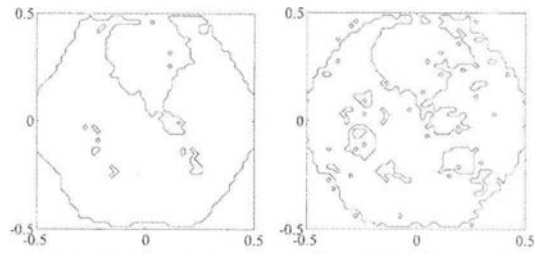


(e) ART under 7 projections

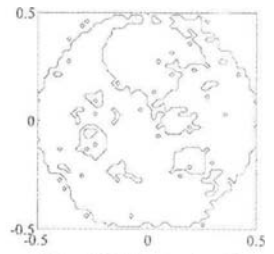


(f) MART under 7 projections

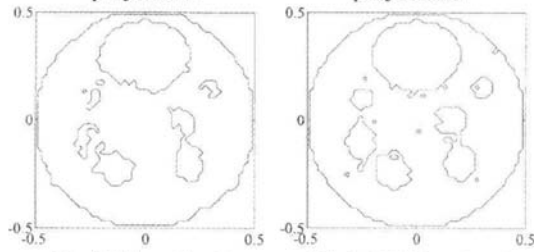
**Fig. 5** Reconstructed fields of annular flow using ART and MART



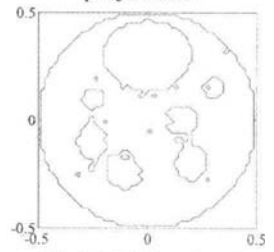
(a) ART under 3 projections



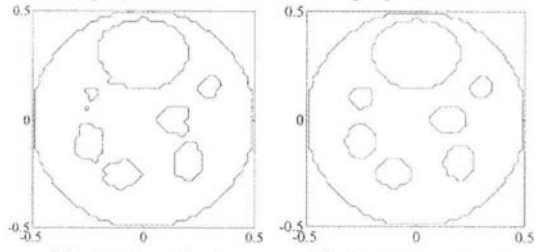
(b) MART under 3 projections



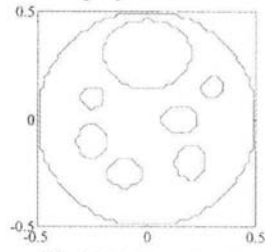
(c) ART under 5 projections



(d) MART under 5 projections



(e) ART under 7 projections



(f) MART under 7 projections

**Fig. 6** Reconstructed fields of bubbly flow using ART and MART

The MART reconstruction of the bubbly flow also shows improvement over the ART in Fig. 6. Both of the ART and the MART reconstructions of the bubbly flow under 3 projections are hardly acceptable because of the excessive artifacts as shown in Figs. 6(a) and (b). Under 5 projections, the ART result also shows the erroneous and noisy data (Fig. 6(c)) whereas the MART result roughly identifies seven bubbles in the density field (Fig. 6(d)). If the number of the projection angle increases, the reconstructions provide definitely more accurate results as shown in Figs. 6(e) and (f). As the case of 5 projections, the MART of 7 projections also calculates better density distributions than that of the ART. The average error appears to be perfect zero percent for the case of 7 projections in Table 1. Thus, the MART with more than 5 projections is appropriate for the case of relatively complex bubbly flow. After tomographic reconstruction, the results of the density distribution are obtained between 0 and 1 instead of only 0 and 1. Thus, the values have been changed to 0 and 1 using the threshold because only two densities of liquid and gas exist in the flow. If the calculated values are not divided into two values, the calculated results

have various values between 0 and 1 as shown in Fig. 7 with the interval of 0.2 (Kihm et al., 1998).

Table 1 presents a comparison of three errors (Eqs. (16) to (18)) for the reconstruction results. The average, rms, and absolute errors are various measures of the reconstruction accuracy for the annular and bubbly flows. These errors are significant when comparing tomographic algorithms using a known reference fields. The reconstruction quality is only estimated by the comparison between the virtual projection  $\hat{\psi}$  and the measured projection  $\psi$  in real experiments because the true field is unknown. For all the tested cases, the reconstruction errors of the MART are lower than those of the ART method.

The number of iterations for the minimum error can be pointed out to stop the iteration step and reconstruct the field at that point (Figs. 8 and 9). Some graphs have been drawn until 1000 iteration steps for x-axis while others drawn until more than 1000 iterations to find the optimum point of the error. Since the error of Fig. 8(a) did not reduce significantly after 1000 iteration steps especially for the MART, the graph was drawn until 1000 iterations for this case. The graphs for Figs. 9(a) and (b) were drawn until 2000 and 4000 iteration steps, respectively because the average error and the reconstructed results did not improve obviously after those iteration steps. The numbers of the iterations of the bubbly flow to reach the minimum errors are larger than those of the annular flow because the shape of the bubbly flow is more complex than that of the annular flow. In comparison of the ART with the MART, the MART approaches the minimum error faster than the ART does as shown in Figs. 8 and 9. If the number of the projection angle increases, the number of the iteration for the minimum error also reduces (Figs. 8 and 9).

The computational times are almost same for the ART and the MART. The computational load depends on the number of the projection angles (the number of the projected data) and the shape of the phantom fields. The computational times of the annular flow for 3, 5, and 7 projection angles are 1 min. 35 sec., 2 min. 38 sec., and 3 min. 42 sec., respectively in the computer with

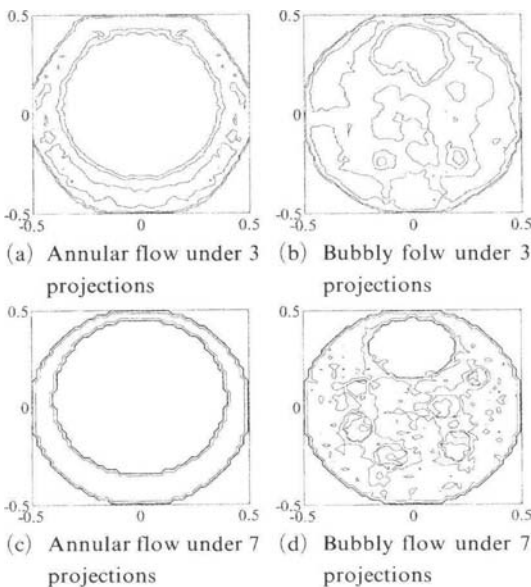


**Fig. 7** Reconstructed fields using MART without adjusting calculated values

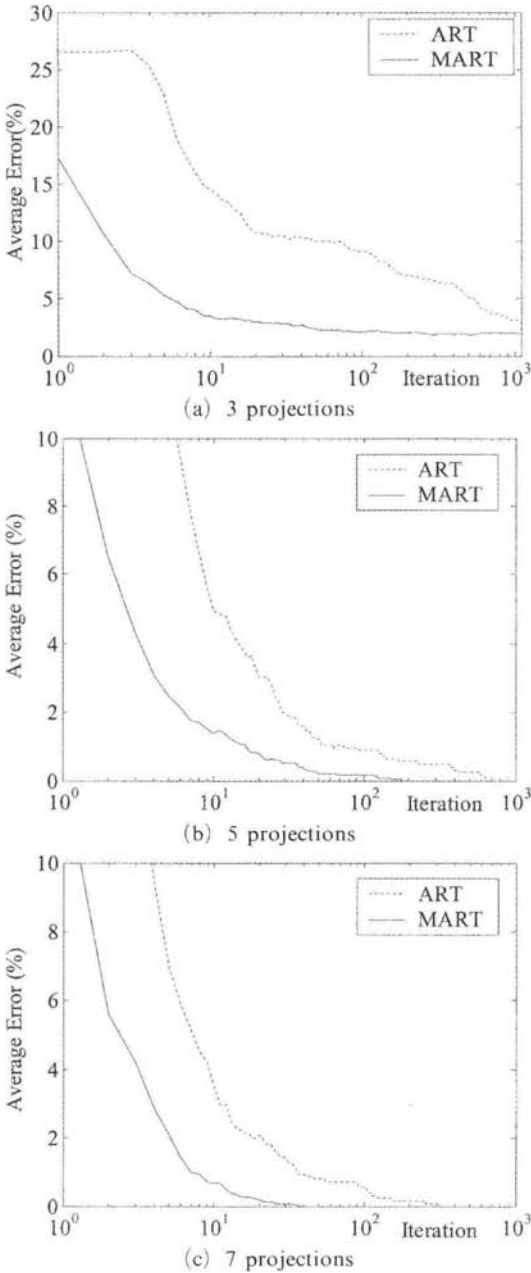


**Fig. 8** Average error versus iteration of ART and MART reconstructions for annular flow

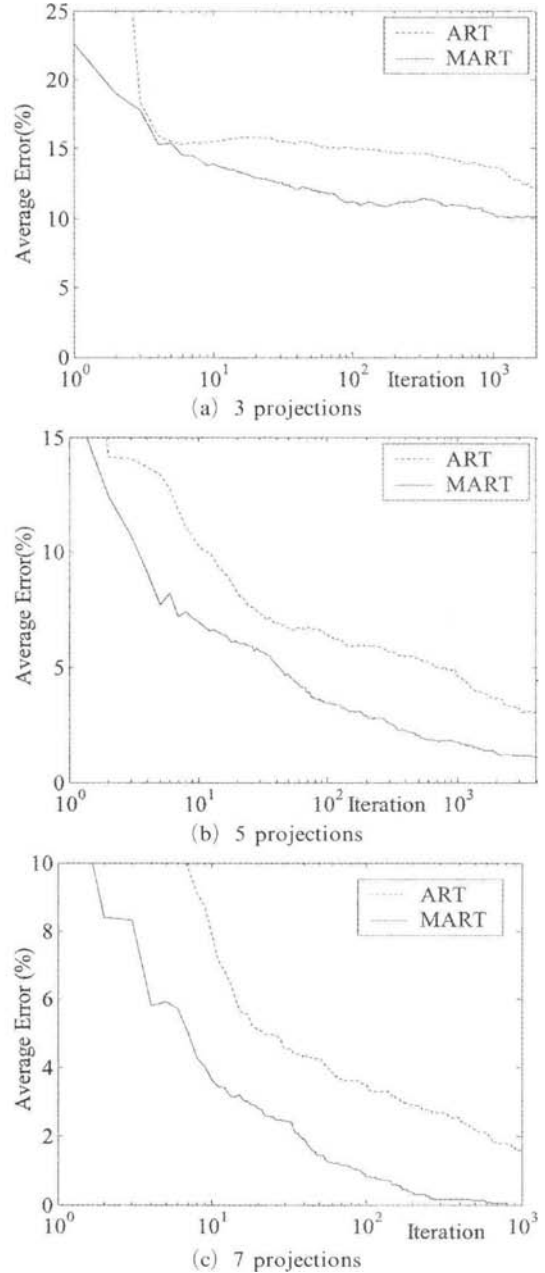


**Fig. 9** Average error versus iteration of ART and MART reconstructions for bubbly flow

the CPU of P4-1.6 GHz and the RAM of 768 Mbytes. The loads of the bubbly flow for 3, 5, and 7 projection angles are 3 min. 32 sec., 5 min. 47 sec., and 8 min. 46 sec., respectively in the same computer. The MART shows better accuracies and less iteration steps as compared with the

ART to reconstruct the bubble images in the two-phase flows.

### 5. Concluding Remarks

The algebraic reconstruction technique (ART)

and the multiplicative algebraic reconstruction technique (MART) have been investigated for the purpose of using tomographic reconstruction of the density distribution of the two-phase flows. The computer synthesized phantom fields such as the annular and bubbly flows have been reconstructed by the ART and the MART to examine the accuracy and efficiency of the methods. In comparison with the ART reconstruction, the MART shows improvement in reconstruction accuracy for the two-phase flows. Also, the MART shows faster convergence of the number of the iteration step to reach the minimum error for the reconstruction of the annular and bubbly flows.

### Acknowledgment

This study was supported by Korea Research Foundation (KRF2001-003-E00009).

### References

- Decker, A. J., 1993, "Tomographic Methods in Flow Diagnostics," *NASA Report*, No. 106330.
- Fomin, N. A., 1998, *Speckle Photography for Fluid Mechanics Measurements*, Springer, Berlin.
- Françon, M., 1979, *Laser Speckle and Applications in Optics*, Academic Press, New York.
- Gordon, R., 1974, "A Tutorial on ART," *IEEE Trans. on Nuclear Science*, Vol. NS-21, pp. 78~92.
- Hanson, K. M. and Wecksung, G. W., 1985, "Local Basis Function Approach to Computed Tomography," *Appl. Opt.*, Vol. 24, No. 23, pp. 4028~4039.
- Kak, A. C. and Slaney, M., 1987, *Principles of Computerized Tomographic Imaging*, IEEE Press, New York.
- Kastell, D., Kihm, K. D. and Fletcher, L. S., 1992, "Study of Laminar Thermal Boundary Layers Occurring around the Leading Edge of a Vertical Isothermal Wall Using a Specklegram Technique," *Exper. Fluids*, Vol. 13, pp. 249~256.
- Kihm, K. D., 1997, "Laser Speckle Photography Technique Applied for Heat and Mass Transfer Problems," *Advan. in Heat Transfer*, Vol. 30, pp. 255-311.
- Kihm, K. D., Ko, H. S. and Lyons, D. P., 1998, "Tomographic Identification of Gas Bubbles in Two-Phase Flows with the Combined Use of the Algebraic Reconstruction Technique and the Genetic Algorithm," *Opt. Lett.*, Vol. 23, No. 9, pp. 658~660.
- Ko, H. S. and Kihm, K. D., 1999, "An Extended Algebraic Reconstruction Technique (ART) for Density-Gradient Projections: Laser Speckle Photographic Tomography," *Exper. Fluids*, Vol. 27, No. 6, pp. 542~550.
- Ko, H. S., Lyons, D. P. and Kihm, K. D., 1997, "A Comparative Study of Algebraic Reconstruction (ART) and Genetic Algorithms (GA) for Beam Deflection Tomography," *ASME Fluids Engrg. Div. Summer Meeting*, Vancouver, Canada, Paper FEDSM 97-3104.
- Ko, H. S., Okamoto, K. and Madarame, H., 2001, "Reconstruction of Transient Three-dimensional Density Distributions Using Digital Speckle Tomography," *Meas. Sci. Tech.*, Vol. 12, No. 8, pp. 1219~1226.
- Liu, T. C., Merzkirch, W. and Oberste-Lehn, K., 1989, "Optical Tomography Applied to a Speckle Photographic Measurement of Asymmetric Flows with Variable Density," *Exper. Fluids*, Vol. 7, pp. 157~163.
- Partington, J. R., 1953, *Physico-Chemical Optics*, Vol. IV, An Advanced Treatise on Physical Chemistry, Longmans Green, London.
- Verhoeven, D., 1993, "Limited-data Computed Tomography Algorithms for the Physical Sciences," *Appl. Opt.*, Vol. 32, No. 20, pp. 3736~3754.
- Vest, C. M., 1979, *Holographic Interferometry*, John Wiley & Sons, New York.